Ultrasonic Wave Propagation in Dissimilar Metal Welds – Application of a Ray-Based Model and Comparison with Experimental Results

Audrey GARDAHAUT [1], Hugues LOURME [1], Frédéric JENSON [1],
Shan LIN [2], Masaki NAGAI [2]

[1] CEA, LIST, Digiteo Labs, Bât. 565, PC 120, F-91191, Gif-sur-Yvette, France
Phone: +33 1 69 08 40 26, Fax: +33 1 69 08 75 97;
E-mail: audrey.gardahaut@cea.fr, hugues.lourme@cea.fr, frederic.jenson@cea.fr
[2] Materials Science Research Laboratory, Central Research Institute of Electric Power Industry,
2-6-1 Nagasaka, Yokohama-shi, Kanagawa-ken 240-0196 Japan;
E-mail: shanlin@criepi.denken.or.jp, nagai@criepi.denken.or.jp

Abstract
Dissimilar Metal Welds (DMW) made of nickel based alloys are widely present in some nuclear power plants at the intersection between the main pipe lines and large components such as the pressure vessel, steam generators and pressurizers. Ultrasonic NonDestructive Testing techniques (NDT) are used in order to maintain the integrity of the primary circuit and detect defects such as Stress Corrosion Cracking (SCC). Nevertheless, disturbances such as beam splitting and skewing may occur due to the anisotropic and inhomogeneous properties of the welding material. These disturbances affect the detection, localization and sizing of possible weld discontinuities. Numerical simulation tools can help to understand these physical phenomena and optimize ultrasonic NDT. A novel ray tracing algorithm has been recently developed in the CIVA platform in order to evaluate the propagation of elastic waves in anisotropic and inhomogeneous media. Based on the solving of two systems of linear ordinary differential equations of the first order, this model allows the evaluation of the ray trajectories and the travel-time, and the computation of the amplitude along a ray tube and in its vicinity. In this approach, the considered medium has to be represented by a smooth description of the elastic properties. This paper presents the work made as part of a collaborative program between CRIEPI and CEA. The ray-based model has been evaluated on a DMW mock-up described thanks to a smooth description of the crystallographic orientation of its constitutive grains. Simulated results of the transmitted beam and the detection of notches located in the weld and the buttering have been compared to experimental measurements performed on this mock-up with phased-array probes.

Keywords: Dissimilar Metal Welds (DMW), Anisotropic and Inhomogeneous Media, Ultrasonic Testing, Ray-Based Approach.

1. Introduction

In worldwide nuclear power plants (NPP), nickel based alloys have been widely used to facilitate the welding of stainless steel cooling line pipes and instrumentation components to the ferritic steel vessels. Some studies [1]-[6] have highlighted the appearance of leaks in dissimilar metal welds (DMW) of the primary circuit due to the occurrence of stress corrosion cracking (SCC) in NPPs. In regard to the safety and the reliability of NPPs, detection and depth sizing of such cracks with high accuracy is a serious issue. Ultrasonic Non Destructive Testing (NDT) techniques are commonly used to control such welded joints located in the primary circuit. However, the interpretation of on-sites inspection of DMWs is particularly difficult due to their internal structures. Indeed, ultrasonic waves can be severely scattered and attenuated because of coarse grains in DMWs and some disturbances of the ultrasonic beam, such as splitting and skewing [7], can be observed due to the anisotropic and inhomogeneous polycrystalline structure of the welds [8]. Consequently, simulation is quite useful to understand the inspection results and those complex phenomena.
Various models have been developed to simulate the ultrasonic propagation such as finite differences [9], finite elements [10, 11] or ray tracing models [12]. Semi-analytical propagation models [13], based on a ray theory, have been implemented in the CIVA software [14, 15], developed by CEA-LIST, and applied to the study of weld inspection. In this case,

the weld is described as a set of several anisotropic homogeneous domains with a given crystallographic orientation. Nevertheless, if the domains have small dimensions compared to the wavelength, the results are valid only if the contrast of impedance between two neighboring media is small [16]. A new modeling approach has been considered in which the weld is described as a continuously variable description of the crystallographic orientation [17]. Based on a Dynamic Ray Tracing (DRT) model, it allows studying the ultrasonic propagation in anisotropic inhomogeneous media.
Therefore, CRIEPI and CEA-LIST both agreed to have a collaborative research program focusing on the understanding of wave propagation in DMWs by means of simulations and experiments, the evaluation of applicability of CIVA to DMWs with complex internal structures and the evaluation of phased array ultrasonic techniques for DMWs inspections.

2. Simulation of the wave propagation in CIVA with the Dynamic Ray Tracing model

The Dynamic Ray Tracing model, usually applied in geophysics [18], is based on the solving of two equations: *the eikonal equation* and *the transport equation* in anisotropic and inhomogeneous media [17].
From the eikonal equation, the following system called axial ray system (1) is obtained:

$$\begin{cases} \dfrac{dx_i}{dT} = a_{ijkl}\, p_l\, g_j^{(m)}\, g_k^{(m)} = V_i^{e(m)}, \\ \dfrac{dp_i}{dT} = -\dfrac{1}{2}\dfrac{\partial a_{ijkl}}{\partial x_i}\, p_k\, p_n\, g_j^{(m)}\, g_l^{(m)}. \end{cases} \tag{1}$$

This system is composed of two coupled ordinary differential equations describing the variations of the position x_i and the slowness p_i with respect to the travel-time $T(x)$. It is written in function of the elastic constants of the medium a_{ijkl}, the density ρ and the components of the slowness vector p_i. $g_j^{(m)}$ are the eigenvectors of the Christoffel tensor corresponding to the polarization vectors and $V_i^{e(m)}$ represent the energy velocity for a mode m. Theirs solutions allow the evaluation of the ray trajectories and the travel-time in the weld.

Called the paraxial ray tracing system, the second system is a system of ordinary linear differential equations of the first order for the paraxial quantities Q_i and P_i and is written as:

$$\begin{cases} \dfrac{d}{dT}\left(\dfrac{dx_i}{d\gamma}\right) = \dfrac{dQ_i}{dT} = \dfrac{1}{2}\dfrac{\partial^2 G}{\partial p_i^{(x)} \partial \gamma}, \\ \dfrac{d}{dT}\left(\dfrac{dp_i^{(x)}}{d\gamma}\right) = \dfrac{dP_i}{dT} = \dfrac{1}{2}\dfrac{\partial^2 G}{\partial x_i \partial \gamma}. \end{cases} \tag{2}$$

This system is expressed in function of γ, representing any parameter of the ray Ω and chosen, for example, as a take-off angle between a reference axis and the initial slowness vector, and the parameter G_m, written as $G_m = a_{ijkl} p_j p_l g_i^{(m)} g_k^{(m)}$, and representing the normalized eigenvalues of the Christoffel tensor. Obtained from the transport equation, it describes the evolution of the ray tube during its propagation and evaluates its amplitude assuming the conservation of the energy across a ray tube section.

Both axial and paraxial ray systems are simultaneously solved by using numerical techniques such as the Euler method in this example. A complete explanation of the dynamic ray tracing model and its solving is provided in [17].

3. Properties of the DMWs – Description of the internal structures

The studied mock-up is a dissimilar V-butt weld, with a welded region and a buttering made of Inconel 600 as represented in Figure 1.

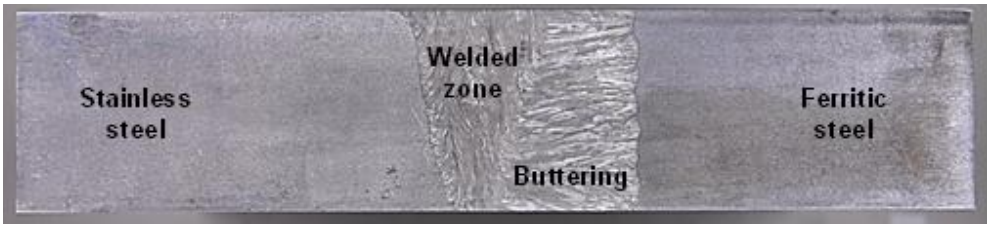

Figure 1: Macrograph of the studied V-butt dissimilar weld.

The welded zone is characterized by an anisotropic and inhomogeneous structure and a significant attenuation. These characteristics are responsible for splitting and skewing of the ultrasonic beam along its propagation. Some input parameters are then needed in order to take those complex phenomena into account in the simulations.

The anisotropy of the materials results of the dependence of the ultrasonic velocity to the direction of propagation and is expressed in the software thanks to the elastic constants. One set of parameters have been found in the literature [19]. Even though these properties are for Inconel 182 and not Inconel 600, they are representative of the anisotropy of the studied V-butt weld and then chosen as input parameters (see Table 1):

	C_{11}	C_{22}	C_{33}	C_{23}	C_{13}	C_{12}	C_{44}	C_{55}	C_{66}	ρ
Inconel 182 [19]	255.8	255.8	236	135.4	137.9	130.5	111.4	111.9	81.4	8260

Table 1: Elastic constants (in GPa) and density (in $kg.m^{-3}$) of Inconel 182.

Caused by the absorption linked to the viscosity of the medium and the scattering of the wave due to the constitutive macroscopic grains, the attenuation represents an energy loss due to the structure of the weld and implies a decrease of the ultrasonic signal. Chassignole *et al.* [19] had evaluated experimentally, with a specific setup, the attenuation coefficient for 316L samples at 2 MHz.

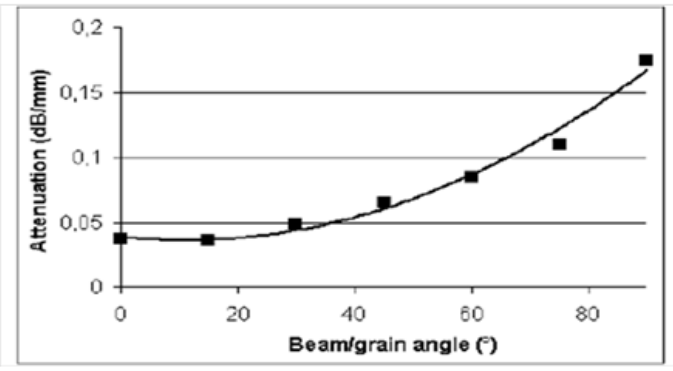

Orientation of the grains	Attenuation (in dB/mm)
0°	0,037
15°	0,036
30°	0,048
45°	0,068
60°	0,087
75°	0,115
90°	0,175

Figure 2: Representation of the attenuation coefficient for L wave at 2 MHz as a function of the orientation of the grains [19].

Figure 2 highlights the link between the attenuation law of the longitudinal wave and the angle between the grain and the incident beam, and gives the values of the attenuation coefficient put in the CIVA software.

The inhomogeneity of the weld depends on its metallurgical structure. As the DRT model is able to evaluate the ultrasonic propagation in anisotropic inhomogeneous media, the variation of the grain orientation has to be defined. To this aim, the weld region is described thanks to a closed-form expression (3) proposed by Ogilvy [12]:

$$\theta = \begin{cases} \arctan\left(\dfrac{T(D + z\tan\alpha)}{x^{\eta}}\right), & for\ x \geq 0, \\ -\arctan\left(\dfrac{T(D + z\tan\alpha)}{(-x)^{\eta}}\right), & for\ x < 0. \end{cases} \tag{3}$$

The parameters D and α are expressed in function of the geometry of the weld while T and η represent the evolution of the orientation of the grain in the weld. The studied V-weld has been considered as symmetrical and the parameters are given in Figure 3. Furthermore, the macrograph highlights that the orientation is the same in all the buttering. It is then described as a homogeneous domain with a grain orientation equal to 78°. The description of the V-butt weld is presented in Figure 3.

$$D = 6.14 \quad \alpha = 12.5$$
$$T = 1 \quad \eta = 1$$

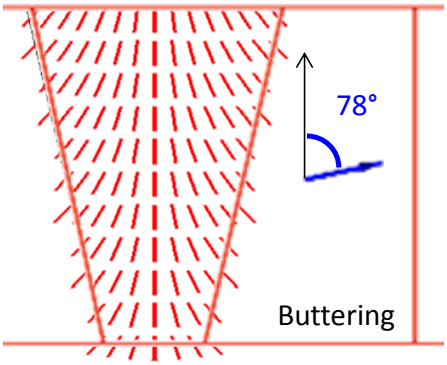

Figure 3: Description of the grain orientation in the studied V-butt weld.

4. Simulated and experimental results of the wave propagation

4.1 Description of the experimentation

The first experiment aimed to measure the propagating field on a plane of the mock-up. The set-up, presented in Figure 4, consists of emitting a longitudinal wave on the top of the specimen with an angle beam transducer and receiving on one side of the mock-up with a normal incidence probe with a 1 mm diameter vibrator. The transmitter and the receiver have a nominal frequency of 2 MHz and the angle beam transducer has a refraction angle equal to 49°.

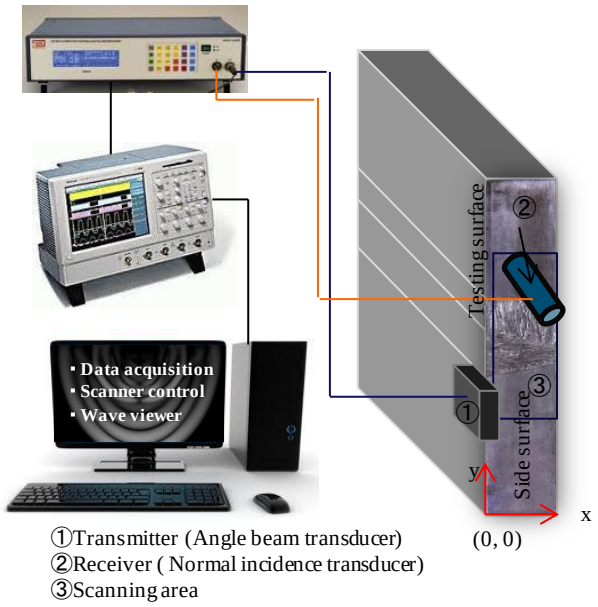

Figure 4: System for wave propagation visualization.

4.2 Results and discussion

The first comparison, shown in Figure 5, is made for an emitting probe positioned on the buttering and a wave propagation made from the ferritic part to the stainless steel one.

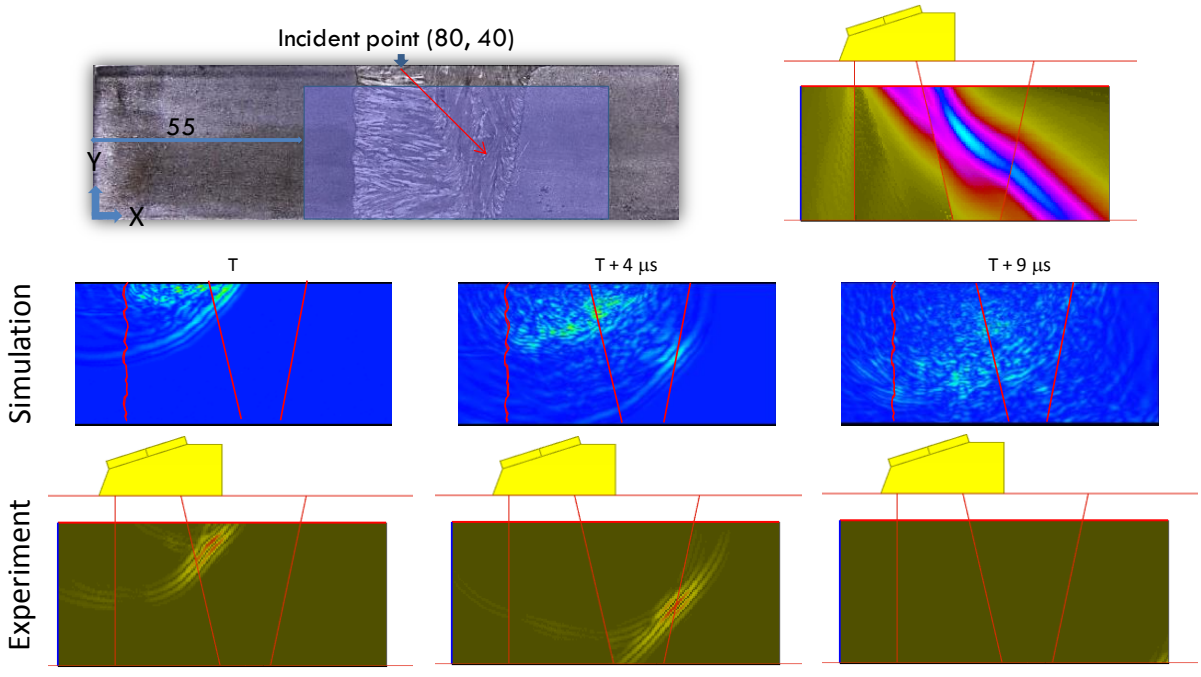

Figure 5: Comparison of experimental and simulated beam of L49° wave for an emitter on the buttering.

At this position, the incident wave is generated in the buttering and propagates in the welding part. The simulated beam module profile highlights that the longitudinal beam, taking into account the inhomogeneity of the region, is deviated at each position of the weld compared to the simulated one in an isotropic medium. The simulated and measured snapshots present a

good agreement at the different chosen time steps. Nevertheless, simulation does not represent the ultrasonic wave field perturbation during the propagation. Indeed, the shear wave has not been taken into account in the simulations and the scattering due to each grains of the weld is not simulated either.

Figure 6 represents the results obtained for an emitter located at the top of the weld for a propagation made from the stainless steel to the ferritic part.

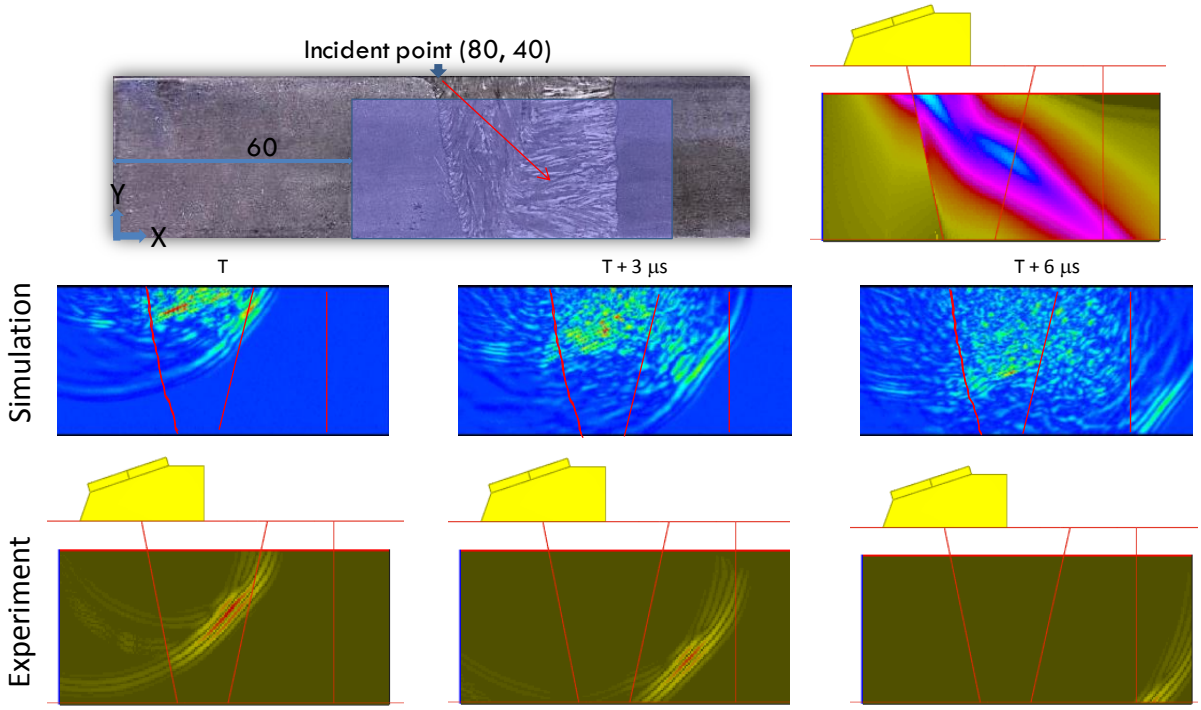

Figure 6: Comparison of experimental and simulated beam of L49° wave for an emitter located on the weld.

In this configuration, the ultrasonic wave is generated at the interface between the ferritic steel and the weld and propagates in the welding zone and in the buttering. Although the simulated wave front is at the same position as the experimental one, we can see that the maximal amplitude positions are slightly different.

5. Inspection simulation: comparison between simulations and experiments

Now that the ability of the model to simulate correctly the transmitted beam has been verified, the simulation of the defect response can be performed. Thus, simulated results are going to be compared to experimental ones.

6.1 Experimental set-up

The aim of this experiment is the detection of three 10 mm height notches located in the buttering (S1), in the weld (S2) and in the stainless steel (S3) as shown in Figure 7. The acquisitions have been made with a 1 MHz linear array transducer of 64 elements (length = 0.5 mm, pitch = 0.6 mm) in a pulse echo technique emitting a longitudinal wave at 49°. The simulations have been performed with CIVA (development version). In the following pictures, T and C indicate the tip diffraction and corner echoes of the defect. The S3 notch, located in the stainless steel, has been chosen as the reference defect. Its corner echo

amplitude is the reference for the S1 and S2 corner echoes whereas its tip echo amplitude is the reference for the S1 and S2 tip echoes.

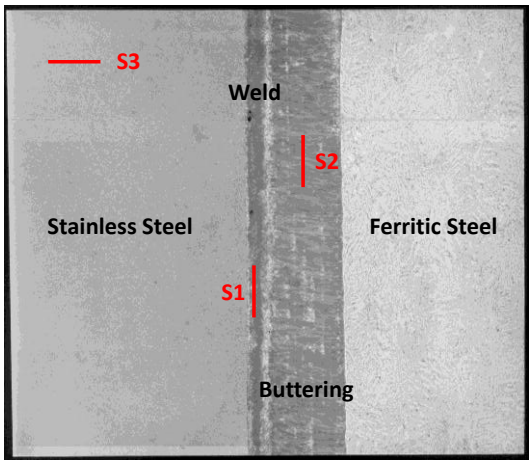

Figure 7: Representation of the location of the three 10 mm height notches in the specimen.

6.2 Comparison of the results and discussion

Figure 8 represents the simulated and measured echoes obtained for an elastic longitudinal wave propagating from the ferritic steel to the stainless steel while Figure 9 is the comparison of experiment and simulation inspection of a wave that propagates from the stainless to the ferritic steel.

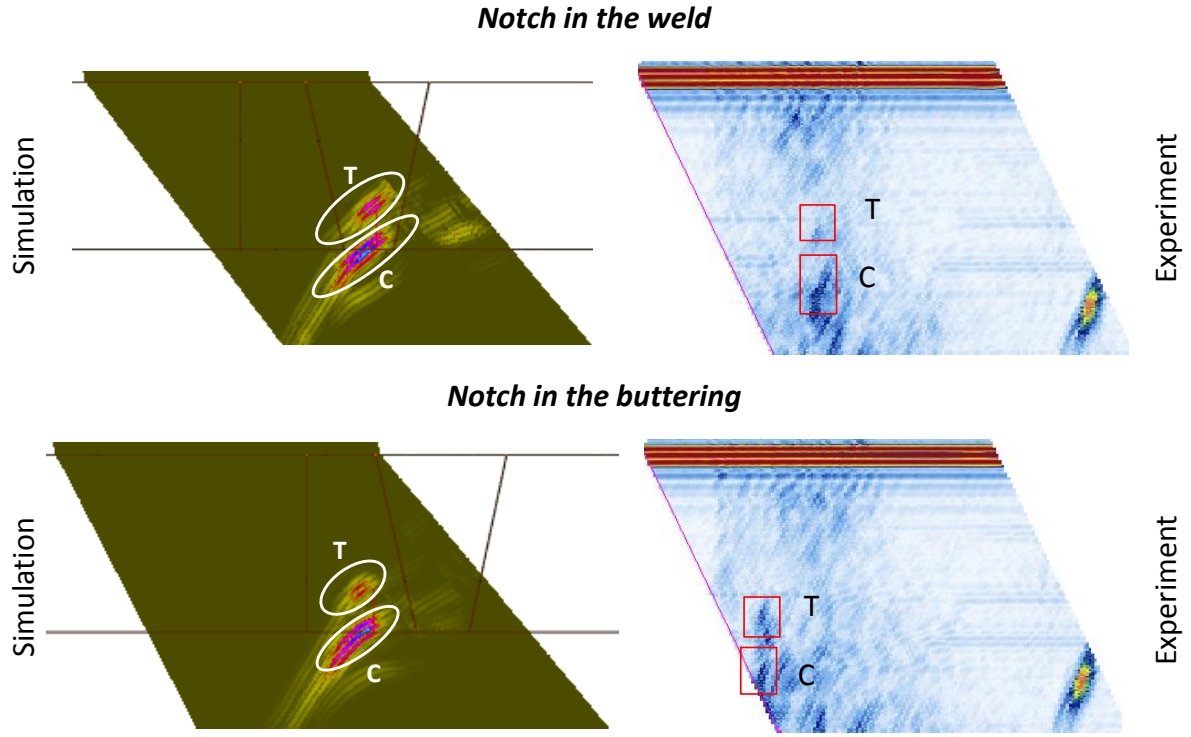

Figure 8: Simulated and experimental inspection of notches located in the buttering and in the weld for a wave that propagates from the ferritic to the stainless steel.

For an ultrasonic propagation from the ferritic steel, tip diffraction and corner echoes of the S1 and S2 notches are well detected in experiments and well reproduced by simulation.

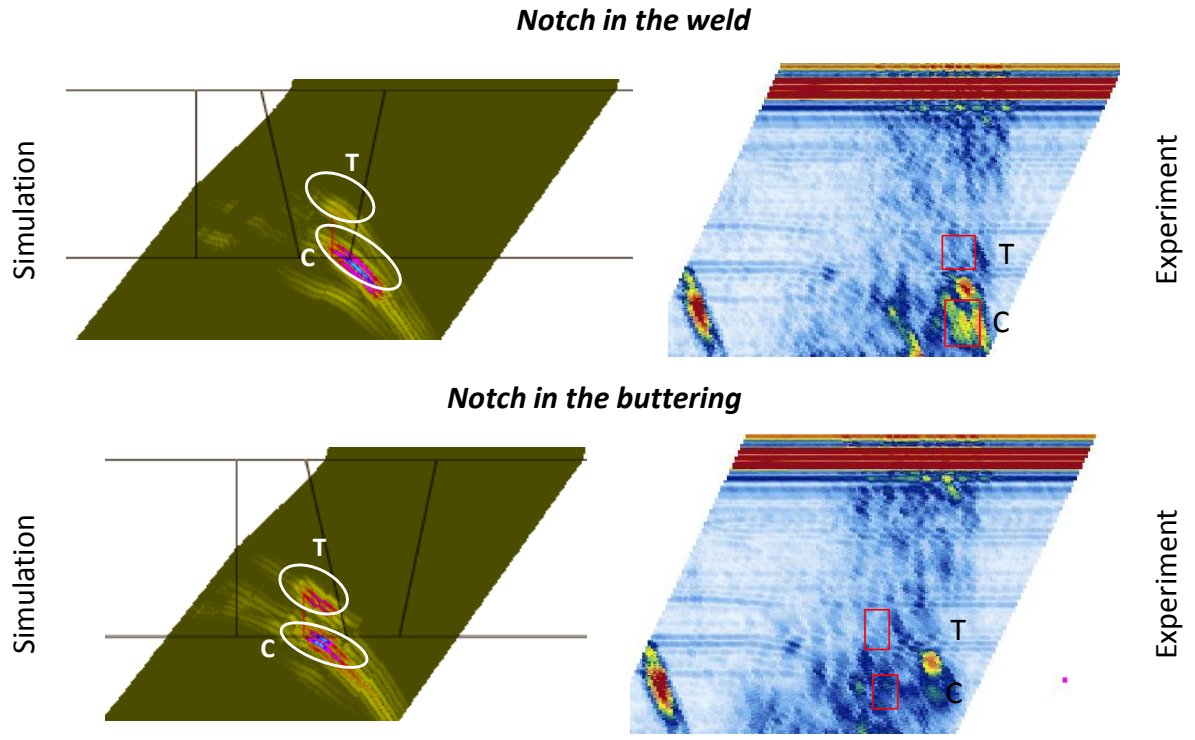

Figure 9: Simulated and experimental inspection of notches located in the buttering and in the weld for a wave propagating form the stainless to the ferritic steel.

In the other direction of propagation, the tip diffraction and corner echoes are well detected in simulation and with difficulty in experiment due to the noise caused by the internal structure of the weld.

The amplitudes of the simulated and measured corner and tip echoes of S1 and S2 notches are given in Table 2 and Table 3 respectively.

		Experiments	Simulation
	Stainless steel (S3)	0	0
Ferritic to stainless steel	Buttering (S2)	-6.3	-5.8
	Weld (S1)	-12.2	-10.1
Stainless steel to ferritic	Buttering (S2)	-14.2	-11.3
	Weld (S1)	-7.0	-3.5

Table 2: Simulated and experimental amplitudes (in dB) of corner echoes for notches S1 and S2.

		Experiments	Simulation
	Stainless steel (S3)	0	0
Ferritic to stainless steel	Buttering (S2)	-2.4	-1.6
	Weld (S1)	-5.6	-2.0
Stainless steel to ferritic	Buttering (S2)	-8.9	-5.7
	Weld (S1)	-5.1	-4.2

Table 3: Simulated and experimental amplitudes (in dB) of tip echoes for notches S1 and S2.

The results in these tables present a very good agreement between simulations and experiments. Indeed, the maximal difference is 3,6 dB when the wave travels through the whole welded zone.

6. Conclusions

This paper has presented simulations and experiments of the ultrasonic propagation and defect response, performed on a V-butt weld, in order to evaluate the applicability of the DRT model developed in CIVA to anisotropic inhomogeneous media. To this aim the welded zone of the studied specimen has been described with a continuously variable representation of the crystallographic orientation obtained thanks to an analytical law.
Firstly, simulations of the ultrasonic propagation through such structures have been compared to the associated experiments. The simulated wave fronts at different time step are well evaluated compared to the experiments. Moreover, simulations of UT inspections of notches located in the buttering and the weld have been performed. The comparisons made with experimental results are in a good agreement.
Nevertheless, slight differences have been highlighted. The evaluation of the amplitude could be improved thanks to an entire continuously variable description of the crystallographic orientation of the weld obtained from the macrograph of the weld. Indeed, this representation would avoid the creation of a straight separation between the buttering and the welded zone. Furthermore, the amplitude is overestimated in simulation. The attenuation used in this work is maybe lower than the real attenuation of the considered material. Last, in the inspection simulation model, the scattering coefficient on the defect is evaluated by taking into account the physical properties of the material on the edges of the defect. In our case, the internal properties of the medium are not the same all over the edges of the defect. The small observed discrepancies may originate from the consideration of these variations of the material properties.

References

1. B G Braatz, S E Cumblidge, S R Doctor and I G Prokofiev, ‘Primary Water Stress Corrosion Cracks in Nickel Alloy Dissimilar Metal Welds: Detection and Sizing Using Established and Emerging Nondestructive Examination Techniques’, IAEA-CN-194-025, pp 1-9, 2012.
2. W H Bamford, L Tunou-Sanjur and R Hsu, ‘Integrity Evaluation for Future Operation: Virgil C. Summer Nuclear Plant Reactor Vessel Nozzle to Pipe Weld Regions’, WCAP-15615, Rev. 0, Westinghouse Engineering, 2000.
3. W H Bamford et al., ‘Alloy 182 Crack Growth and its Impact on Service-Induced Cracking in PWR Plant Piping’, (Proc. 10th International Conference on Environmental

Degradation of Materials in Nuclear Power Systems – Water Reactors, Houston, Texas), NACE. Paper 34, 2002.
4. A Jenssen et al., 'Assessment of Cracking in Dissimilar Metal Welds', (Proc. 10th International Conference on Environmental Degradation of Materials in Nuclear Power Systems – Water Reactors, Houston, Texas), NACE, 2002.
5. A Jenssen et al., 'Structural Assessment of Defected Nozzle to Safe-End Welds in Ringhals-3 and -4', (Proc. Fontevraud V Intl. Symp.), SFEN, 2000.
6. S E Cumblidge et al., 'Nondestructive and Destructive Examination Studies on Removed from-Service Control Rod Drive Mechanism Penetrations', NUREG/CR-6996; PNNL-18372, U.S. Nuclear Regulatory Commission, Washington, D.C., 2009.
7. B Chassignole, O Dupond, L Doudet, V Duwig and N Etchegaray, 'Ultrasonic Examination of Austenitic Weld: Illustration of the Disturbances of the Ultrasonic Beam', 35th Review of Progress in Quantitative Nondestructive Evaluation, Vol. 28, pp 1886-1893, 2009.
8. D S Kupperman and K J Reimann, 'Ultrasonic wave propagation and anisotropy in austenitic stainless steel weld metal', IEEE Transactions on Sonics and Ultrasonics, Vol. SU-27, No 1, pp 7-15, 1980.
9. P Fellinger, R Marklein, K J Langenberg and S Klaholz, 'Numerical Modeling of Elastic Wave Propagation and Scattering with EFIT – Elastodynamic Finite Integration Technique', Wave Motion, Vol. 21, pp 47-66, 1995.
10. A Apfel, J Moysan, G Corneloup, T Fouquet and B Chassignole, 'Coupling an Ultrasonic Propagation Code with a Model of the Heterogeneity of Multipass Welds to Simulate Ultrasonic Testing', Ultrasonics, Vol. 43, pp 447-456, 2005.
11. B Chassignole, V Duwig, M-A Ploix, P Guy and R El Guerjouma, 'Modelling the Attenuation in the ATHENA Finite Elements Code for the Ultrasonic Testing of Austenitic Stainless Steel Welds', Ultrasonics, Vol. 49, pp 653-685, 2009.
12. J A Ogilvy, 'Computerized Ultrasonic Ray Tracing in Austenitic Steel', NDT International, Vol. 18, No 2, pp 67-77, 1985.
13. N Gengembre and A Lhémery, 'Pencil Method in Elastodynamics: Application to Ultrasonic Field Computation', Ultrasonics, Vol. 38, pp 495-499, 2000.
14. CIVA software platform for simulating NDT techniques (UT, EC, RT) http://www-civa.cea.fr
15. A Lhémery, P Calmon, I Lecœur-Taïbi, R Raillon and L Paradis, 'Modeling Tools for Ultrasonic Inspection of Welds', NDT&E International, Vol. 37, pp499-513, 2000.
16. K Jezzine, A Gardahaut, N Leymarie and S Chatillon, 'Evaluation of Ray-Based Methods for the Simulation of UT Welds Inspection', 39th Review of Progress in Quantitative Nondestructive Evaluation, Vol. 32B, pp 1073-1080, 2013.
17. A Gardahaut, K Jezzine and D Cassereau, 'Paraxial Ray-Tracing Approach for the Simulation of Ultrasonic Inspection of Welds', 39th Review of Progress in Quantitative Nondestructive Evaluation, Vol. 33A, pp 529-536, 2014.
18. V Červený, 'Seismic Ray Theory', Cambridge: Cambridge University Press, 2001.
19. B Chassignole, O Dupond and L Doudet, 'Ultrasonic and metallurgical examination of an alloy 182 welding mold', 7th International Conference on NDE in Relation to Structural Integrity for Nuclear and Pressurized Components, 12-15 May, Yokohama, Japan, 2009.